# Influence of Seed structure on Volume distribution of $\alpha$-Synuclein Oligomer at Early Stages of Aggregation using nanopipette

Saly Charles-Achille, Jean-Marc Janot, Bastien Cayrol, Sebastien Balme

ChemBioChem

Research Article
doi.org/10.1002/cbic.202300748

Chemistry Europe
European Chemical Societies Publishing

www.chembiochem.org

# Influence of Seed structure on Volume distribution of α-Synuclein Oligomer at Early Stages of Aggregation using nanopipette

Saly Charles-Achille,[a] Jean-Marc Janot,[a] Bastien Cayrol,[b] and Sebastien Balme*[b]

Understanding α-synuclein aggregation is crucial in the context of Parkinson's disease. The objective of this study was to investigate the influence of aggregation induced by preformed seeding on the volume of oligomers during the early stages, using a label-free, single-molecule characterization approach. By utilizing nanopipettes of varying sizes, the volume of the oligomers can be calculated from the amplitude of the current blockade and pipette geometry. Further investigation of the aggregates formed over time in the presence of added seeds revealed an acceleration in the formation of large aggregates and the existence of multiple distinct populations of oligomers. Additionally, we observed that spontaneously formed seeds inhibited the formation of smaller oligomers, in contrast to the effect of HNE seeds. These results suggest that the seeds play a crucial role in the formation of oligomers and their sizes during the early stages of aggregation, whereas the classical thioflavin T assay remains negative.

## Introduction

α-Synuclein is an intrinsically disordered protein involved in the pathogenesis of Parkinson's disease (PD) and other synucleinopathies.[1] The aggregation can be divided into three stages. The first phase, known as the lag phase, is the initial stage of oligomer formation. It is characterized by a negative thioflavin T (ThT) assay before exponential growth of fibrils.[2] It is characterized by a very slow nucleation growth rate, in which monomers coexist with small, soluble transient oligomers.[3] Oligomers produced during the lag phase are considered the most toxic species and vary in size, structure, and morphology. Oligomers produced during the lag phase are often difficult to characterize owing to their heterogeneity and transient nature.[4] This necessitates the development of an innovative approach based on the label-free single-molecule characterization of samples with continuous measurements.

Seeding accelerates the nucleation process by adding preformed aggregates to the monomers.[5] They can be generated from mature fibers sonicated into shorter fibrils[6] or by large, stable oligomers.[7] The species from which α-synuclein seeds are generated influences seeding rate.[8] For example, when human α-synuclein is seeded with A53T aggregates, straight fibrils with short protease-resistant cores are formed.[9] Oligomers induced by 4-Hydroxy-2-Nonenal (HNE) are capable of initiate the formation of amyloid fibrils from monomeric α-synuclein under in vitro conditions.[10] The formation of α-synuclein amyloid fibrils is accelerated in the presence of preformed lysozyme and insulin fibril seeds via a cross-seeding process.[11] The formation of β-sheet-rich neurotoxic tau oligomers has also been observed in vitro due to the cross-seeding effect of α-synuclein.[12] In addition to its effect on the aggregation mechanism and kinetics, seeding plays a crucial role in the real-time quaking-induced conversion (RT-QUIC) technique, which is currently being developed for diagnosis.[13] The limitations of this approach are the time and monomer concentration that are intrinsically linked to the detection method. Specifically, the fluorescence of ThT requires conversion of a sufficient number of monomers into amyloid-rich β-sheet structures. However, this time can be significantly reduced through single-molecule detection using confocal fluorescence spectroscopy and utilization of mutant monomers.[14]

Among single-molecule sensing, biological nanopores are an emerging one that is particularly relevant for the investigation of protein assembly, mutation, or post-translational modification.[15] On the other hand the utilization of solid-state nanopore technology has proven to be highly effective for the detection of protein aggregates using the resistance pulse method.[16,17] This label-free method involves the application of a continuous voltage across a nanometer-sized aperture filled with an electrolyte solution to record the resulting ionic current over time. The passage of a protein aggregate induces fluctuations in the current signal, and the characteristics of these fluctuations are linked to the properties of the aggregate, such as its size, charge, or diffusion coefficient. Various solid-

[a] S. Charles-Achille, J.-M. Janot
Institut Européen des Membranes, UMR5635 University of Montpellier ENCSM CNRS, Place Eugène Bataillon, 34095 Montpellier cedex 5, France

[b] B. Cayrol, S. Balme
PHIM Plant Health Institute, Univ Montpellier, INRAE, CIRAD, Institut Agro, IRD, 34000 Montpellier, France
E-mail: sebastien.balme@umontpellier.fr

Supporting information for this article is available on the WWW under https://doi.org/10.1002/cbic.202300748

state nanopores have been used to detect aβ and α-synuclein aggregates.[16] Nanopores with a low aspect ratio, typically composed of SiN and functionalized to prevent fouling, have been shown to offer the best resolution, as recently demonstrated in the case of α-synuclein.[18] Their sensitivity allows the differentiation of several populations of oligomers produced during aggregation.[19] It has also been used to compare the composition of oligomers between mutants and the wild-type.[20] Despite their high resolution, the production and functionalization of SiN nanopores are challenging, leading to a low success rate across all experimental steps. Conversely, nanopores with asymmetrical geometry and high aspect ratio, obtained through the track-etching technique of polymer films or laser-pulled quartz nanopipettes, offer long lifetimes and are easy to design. In addition, their asymmetrical shape allows the detection of fibrils.[21,22] They have been used to detect various protein aggregates and amyloids, including β-lactoglobulin,[23] lysozyme,[24] tau,[25] aβ,[26] and α-synuclein,[27] at different stages of aggregation. They have also been successfully used to characterize the effects of enzyme degradation.[28] Among the high-aspect-ratio nanopores, nanopipettes offer an interesting platform for amyloid sensing. They were composed of a reservoir of 10 μL and a tunable sensing zone ranging from a few nanometers to micrometers. Using these nanopores, we recently demonstrated good agreement between the recorded signal and the volume of the fiber and small oligomers of aβ-42 using a simple geometric model.[22] On the other hand, the nanopipette allows us to follow the aggregation induced by the addition of seeds through an innovative technique called real-time fast amyloid seeding and translocation (RT-FAST).[29,30] The latter, which is suitable for α-synuclein and aβ-42, shows promise for further development of diagnostic tools. It also allows for the investigation of aggregation at an early stage, enabling evaluation of the volume of each detected oligomer.

Following the proof-of-concept of RT-FAST, we propose to further enhance the method by providing size information about the oligomer produced during the early stage of aggregation. The primary objective of the present study was to develop a strategy for determining the size of oligomer species. To achieve this objective, we calibrated a series of nanopipettes of varying diameters using two solutions of α-synuclein oligomers. Our aim was to propose a straightforward geometrical model that could be used to determine the volume of oligomers based on the amplitude of the current blockade. We then applied the model to investigate the impact of seeds with different morphologies on the volume of oligomers during the early stage of aggregation under continuous measurements. To this end, a series of experiments using RT-FAST were proposed, in which α-synuclein aggregates were seeded with fibrillar and non-fibrillar oligomers. The goal of this second part was to provide, for the first time, a map of oligomer size at an early stage (less than 6 h) measured fly-by, regardless of their structure and without the use of labels.

## Results and Discussion

### Geometrical model to estimate oligomer volume

The first objective of this study was to propose an approach for deducing the volumes of oligomers from the amplitudes of the current blockades. To this end, two types of α-synuclein oligomers produced by ND Biosciences were used.[31] The oligomers obtained through spontaneous aggregation (SP) had a size distribution ranging from 10 to 37 nm, whereas those incubated with dopamine (DA) were smaller, measuring between 8 nm and 22 nm. The supplied data were confirmed by TEM at the end of our nanopore experiments to ensure that their sizes did not change during the experiments (Figure SI-2). Both types of oligomer solutions were analyzed using several nanopipettes with diameters ranging from 10 to 50 nm to map all the oligomers present in the solution (see Table SI-2). In general, biomolecules can be detected by nanopores either by applying an electroosmotic force (EOF) with a voltage greater than 0 V or, more classically, by applying an electrophoretic force (EF).[32] At pH 7.4, α-synuclein became negatively charged on the quartz surface of the pipette following plasma activation. This was confirmed by the rectification of the ionic current observed when a positive voltage was applied ( Figure SI-1). Thus, in our device, when a negative voltage is applied to a reservoir containing α-synuclein oligomers, the latter are driven towards the nanopore by an electrophoretic force. Conversely, when a positive voltage is applied, cation transport within the electrical double layer causes the solution to flow out of the nanopores. This, in turn, creates an electroosmotic driving force for the analyte. Examples of current traces obtained for the detection of α-synuclein oligomers using nanopores of various diameters are shown in Figure 1. The traces recorded for voltages of +500 mV (EOF) and −500 mV (EF) show current blockages induced by the oligomer, regardless of the diameter of the nanopore. In addition, when EF was applied, the capture rate was greater than that EOF was applied. This first result demonstrates that the oligomers are more easily translocated towards the detection zone of the pipette under the influence of the electric field. However, we only observed that for nanopores smaller than 25 nm, clogging under a negative voltage could be attributed to the presence of larger aggregates in the sample. However, by applying electroosmotic flow, this clogging phenomenon does not occur. This can be interpreted by the fact that the less charged and smaller oligomers move more easily towards the sensing zone of the nanopipette than the larger and, therefore, more charged ones. This leads to a drop in the capture rate, as is generally reported, but is also a type of'electroselection' in our case. In summary, electrophoretic force is the most suitable method for detecting oligomers. However, a disadvantage of this approach is that it can cause clogging of the small pipette when dealing with oligomers larger than the nanopores. It is preferable to avoid nanopore clogging over time when studying the aggregation kinetics. Our aim was to map all oligomer species using a wide range of nanopipette diameters. Consequently, we continued

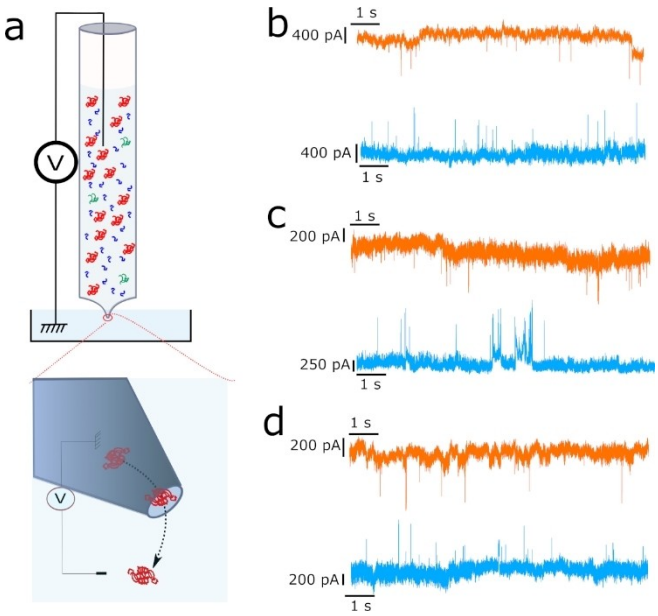


**Figure 1.** a) Sketch of α-synuclein oligomers detection using nanopipette. Typical current trace obtained during the detection of α-synuclein oligomers (SP) and (DA) using nanopipette with diameter b 39 nm, c 22 nm, d 19 nm by applied + 500 mV (orange trace) or −500 mV (bleu trace). These current traces were recorded using the following condition NaCl 1 M, PBS 1X, the base line was not corrected.

our investigation by applying electroosmotic flow (+500 mV), even though the capture rate was lower.

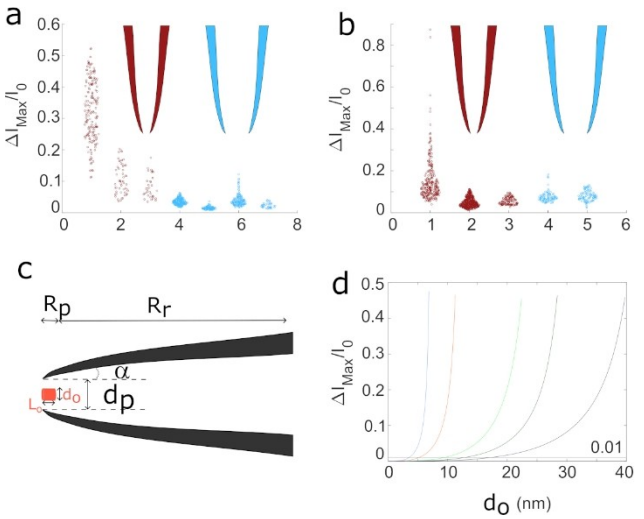


**Figure 2.** a) Distribution of the $\Delta I_{max}/I$ recorded for the α-synuclein SP oligomers using small (red) nanopipettes (diameter 5 nm, 7 nm, 9 nm respectively) and using large (blue) nanopipettes (diameter 20 nm, 28 nm, 39 and 40 nm respectively). b) Distribution of the $\Delta I_{max}/I$ recorded for the α-synuclein DA oligomers using small (red) nanopipettes (diameter 9 nm, 11 nm and 12 nm respectively) and using large (blue) nanopipettes (diameter 20 nm and 22 nm respectively). c) Scheme of the nanopore geometry used for the equations 2 to 6. d) Simulations of $\Delta I_{max}/I$ using equations 6 and 7 as a function of the $2r_0$, considering nanopipette with diameter 9 nm (bleu), 12 nm (orange), 16 nm (light green), 30 nm (dark green) and 57 nm (violet).

Figure 2 illustrates the distribution of $\Delta I_{max}/I$ measured during the translocation of the two types of oligomers into nanopores of varying diameters. These distributions were dispersed, indicating polydispersity of the samples. However, contrary to the findings reported by Awasthi et al.,[18] the use of a nanopipette did not allow for a clear distinction between the different oligomer populations when considering nanopores with diameters ranging from 26 nm to 50 nm. This limitation in the resolution of the nanopore can be attributed to the conical geometry and the high aspect ratio of the nanopipette. To substantiate this, we simulated the expected blocking amplitudes for aggregates of different volumes using a straightforward geometric model. Specifically, we considered the resistance of the nanopore with an oligomer to be the sum of the resistance $R_{max}$ (as shown in Figure 2c).

$$R_{\max} = R_p + R_r = \frac{1}{G_r} + \frac{1}{G_p} \tag{1}$$

$R_p$ corresponds to the resistance of the sensing zone of the nanopipette, which is partially obstructed by an oligomer. Therefore, it depended on the radius ($r_p$) and angle (α) of the pipette determined for each nanopipette and the volume ($V_o$) of the oligomer. To simplify the problem, the latter was considered as a cylinder of length ($L_o$) and radius ($r_o$) for those $L_o = 2r_o$

with a radius equal to the length of *x*, placed exactly at the nanopipette aperture, and centered on the x-axis (see Figure 2c). $R_r$ corresponds to part of the nanopipette that is free of oligomers. The resistance is expressed as follows:

$$R_r = \frac{1}{G} - \frac{L_o}{\kappa\pi r_p\left(r_p + (2r_0)a\right)} \quad \text{with} a = < zs > \tag{2}$$

In equation 3, the first term G is the nanopore conductance without aggregates. The second term is related to the nanopore entrance in the oligomer. It is defined by the radius of the nanopipette and length $L_o$ of the oligomer. It should be noted $R_p^{empty}$ is free and $R_p$ is occupied within oligomers. The latter can be defined from the adaptation of ref[33] as

$$G_p = G_p^{\text{empty}}\left(1 - \frac{V_o}{V_p}\right) \tag{3}$$

Where $V_o$ and $V_p$ are the volumes of the oligomer and the sensing zone of the nanopore, respectively. By including the eqs. 2 and 3 in the eq. 1,

$$R_{\max} = \frac{1}{\left(\kappa\pi r_p\left(r_p + 2r_0a\right)/2r_0\right) -} - \left(1 - \left(r_0^2/2r_p\left(r_p + 2r_0a\right)\right)\right) \frac{1}{G} - \frac{2x}{\kappa\pi r_p\left(r_p + (2r_0)a\right)} \tag{4}$$

Finally the $\Delta I_{max}/I$ is obtained by the following relation eq. 5

$$\frac{\Delta I_{max}}{I} = \frac{G^{-1}}{G^{-1} - R_{max}} \quad (5)$$

The simulations reported in Figure 2d show that a nanopore can only discriminate a small fraction of oligomers when the detection threshold is set at 1% of the current. Specifically, for a set of representative experimental nanopipettes with diameters of approximately 10 nm, 20 nm, and 40 nm, only oligomers larger than 5 nm, 15 nm, and 26 nm were detected. This refers to oligomer sizes that are larger than the radius of the nanopore. The simulation confirmed that the nanopipette had a limited range of size detection compared to the low-aspect-ratio nanopore. Additionally, it confirms that analysis using pipettes of various sizes can provide comprehensive information on the volume of oligomers present in a sample. We noticed that a nanopore with a low aspect ratio (SiN) also required a set of diameters ranging from 25 nm to 56 nm to size oligomers up to 5000 $nm^3$.[18]

Using the geometric approach described above, we calculated the equivalent volume of each oligomer. Briefly, we deduced the $R_{max}$ of the events from the $\Delta I_{max}/I$ and the $G$ using equation 6. Then, equation 5 is solved for each value of $R_{max}$ to find the value of $r_o$ and finally calculate the volume $V_o$. The results obtained from the seven nanopores used to characterize the SP oligomers and the five nanopores used to characterize the DA oligomers were combined, and the distribution histogram is plotted in Figure 3. For SP oligomers, the distribution of oligomer volumes obtained with nanopores with diameters greater than 10 nm was found to be between 100 $nm^3$ and 2000 $nm^3$ and between 5000 $nm^3$ and 25000 $nm^3$ when a larger nanopore was used. To estimate the order of magnitude of the oligomer size, we calculated the size, $L_o$ of the cylinder. It is clear that this size is not exact because we cannot state about the exact oligomer geometry. These measured volumes corresponded to oligomer sizes $L_0$ ranging from 5 to 30 nm, which is consistent with the data provided by the supplier. We also note that the distributions are multimodal, allowing us to determine peaks centered at 150 $nm^3$, 780 $nm^3$, and 4545 $nm^3$, 9670 $nm^3$ by combining the results obtained with different nanopores corresponding to sizes $L_0$ of 6 nm, 10 nm, 18 nm, and 23 nm.

Analysis of the DA oligomers revealed a smaller size distribution than typical SPs, with a volume distribution ranging from 150 $nm^3$ to 5000 $nm^3$, corresponding to sizes between 6 nm and 19 nm. Further analysis revealed two populations, one centered around 341 $nm^3$ and the other at 2866 $nm^3$, corresponding to oligomer sizes of 8 nm and 15 nm, respectively. The latter result also agrees with the supplier's data. In this section, we demonstrate that a straightforward geometric model can be utilized to estimate the diameter of oligomers based on the amplitude of the current blockade and the pore geometry, including its diameter and angle. However, unlike nanopores with low aspect ratios, nanopipettes are not efficient in detecting a wide range of oligomer sizes, particularly small ones. By using pipettes of different diameters and combining the results, it is possible to analyze complex samples and determine various populations. The simplicity and low cost of nanopipette fabrication make it a feasible option. Additionally, the application of an electroosmotic force allows for the use of nanopore diameters smaller than the size of the oligomers while minimizing the occurrence of clogging.

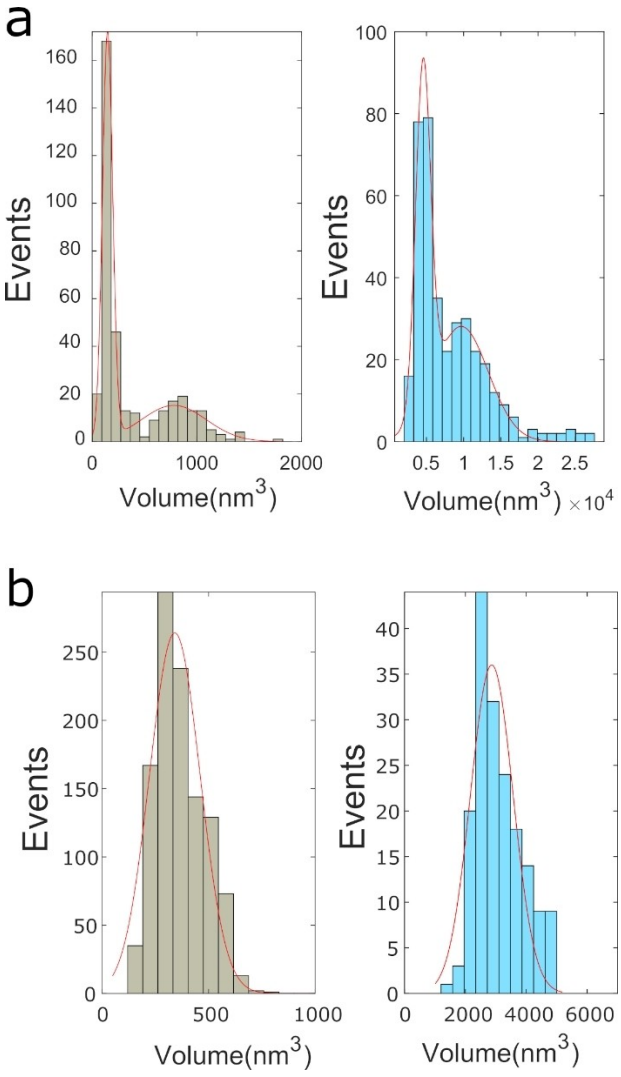


**Figure 3.** Distribution of a) SP and b) DA oligomer volume deduced from the $\Delta I_{max}/I$ and the equations 6,7. The red line is the Gaussian fit of the distribution.

### Impact of seed structure on the aggregation of α-Synuclein

In the previous section, we validated a method for characterizing a mixture of oligomers by combining a geometric model and an analysis using nanopores of different diameters. In this section, we employ this approach to investigate the impact of incorporating seeds on the size distribution of α-synuclein aggregates over time. Specifically, we aimed to determine the influence of seed morphology on oligomer formation during the early stages of aggregation, when the ThT signal was negative.

The characterization of the aggregates formed over time was followed by RT-FAST. These experiments involved incubating α-synuclein monomers directly in the reservoir of a nanopipette at a concentration of 100 nM. Two conditions were tested: one without preformed seeds (control) and the other with 200 pM (Eq. monomer) of seeds. The oligomers formed were analyzed on the nanopore sensor by applying an EOF (V = 500 mV) every 30 min for 360 min to obtain information on the formation time of the different populations of aggregates as well as their size. For each condition, the RT-FAST experiments were carried out with nanopipettes ranging in diameter from 10 nm to 45 nm (Figures 4 and SI-3, 4). The seeds used for this application were obtained through spontaneous aggregation of α-synuclein monomers at two different time points: 6 h and 23 h. TEM imaging showed that after 6 h of aggregation, the solution mainly contained oligomers with a nonfibrillar structure, as confirmed by a negative response to the ThT assay. After 23 h of incubation, the signal was positive for ThT, and TEM revealed a heterogeneous sample consisting of spherical oligomers and fibrillar structures. The latest seeds containing HNE that were used in this study exhibited a homogeneous fibrillar structure. However, they remain soluble in water even though their structures are mostly composed of β-sheets.[10,34]

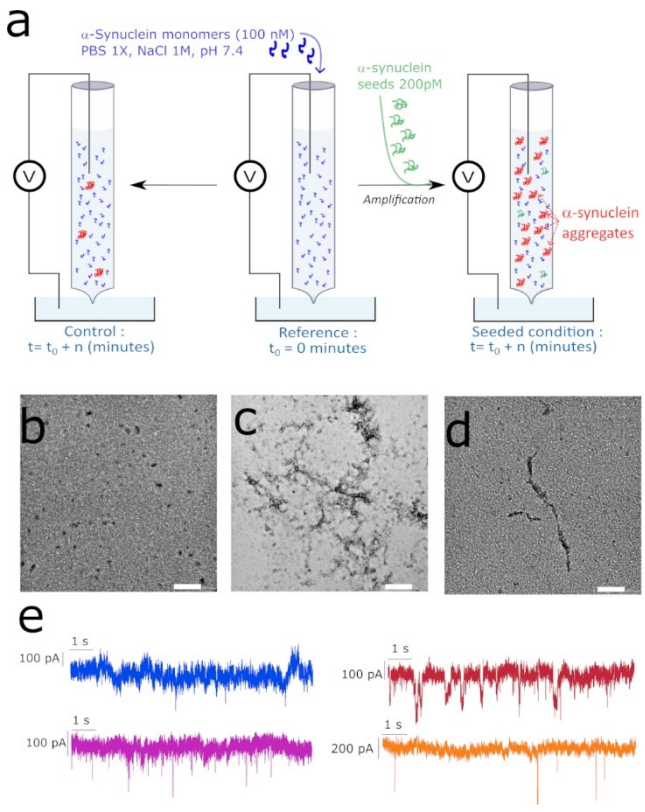


**Figure 4.** a) Sketch of RT-FAST experiments. TEM of b) oligomers obtained after 6 h of incubation, c) fibrils obtained by incubation with HNE d) fibrils obtained after 24 h of incubation. e) Examples of current trace obtained after 210 min of incubation for the control (blue), the experiment performed by adding seeds oligomers (red), fibril-HNE (pink), and fibrils (orange). For TEM image the scale bare is 200 nm. The baseline values are 6.75 nA, 6.6 nA 6.15 nA and 5.6 nA for the control (blue), the experiment performed by adding seeds oligomers, fibril-HNE, and fibrils.

We have also controlled the presence of oligomers at the end of incubation under all RT-FAST condition time by TEM (Figure SI-5).

The control experiment, which investigated aggregate formation in the absence of seeds, was replicated using nine nanopipettes (Table SI-3). Figure 5a depicts the volume distribution of the oligomers detected over time. These results reveal the existence of two distinct populations. The smaller population consisted of oligomers with volumes of less than 1000 $nm^3$ and diameters greater than 15 nm. This population was detected after a 30-minute incubation period. This population corresponded to spontaneously formed oligomers with sizes smaller than 10 nm. A larger population of oligomers with a volume range of 1000 $nm^3$ to 4000 $nm^3$ (diameter between 10 and 17 nm) appeared only after a 120-minute incubation period. The oligomer sizes measured are in agreement with those previously characterized and are consistent with literature reports.[7,35] The first series of experiments revealed a non-monomodal distribution of oligomers, indicating heterogeneous mixing during the lag phase (negative ThT assay signals). These findings are consistent with those of previous studies showing the polymorphic nature of α-synuclein oligomers.

Figure 5b and c depict the distributions of oligomer formation upon the addition of non-fibrillar and fibrillar seeds, respectively. In both cases, aggregates with volumes exceeding 1000 $nm^3$ were detected within 30 min of incubation. This finding emphasizes the role of seeds in accelerating the formation of this type of oligomer. In contrast, the control exhibited a non-monomodal volume distribution of the oligomers, indicating the presence of multiple distinct species. Further examination of the results revealed significant discrepancies depending on the seed added. Specifically, the addition of non-fibrillar oligomers led to the rapid formation of oligomers with a volume greater than 1000 $nm^3$, whereas the addition of fibrillar seeds led to the formation of smaller

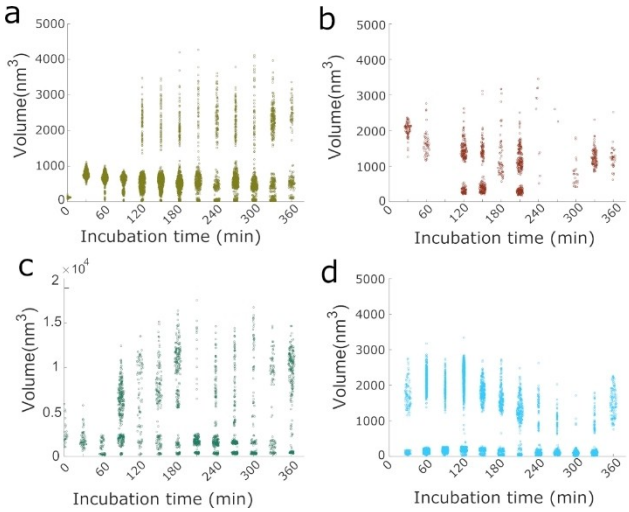


**Figure 5.** Distribution of oligomer volume detected by nanopore with diameters from 10 nm to 50 nm as a function of incubation time for a) the control (light green) the experiment performed by adding seeds, b) oligomers (brown), c) fibrils (green) and d) fibril-HNE (blue).

oligomers. As the incubation time increased, the distribution of oligomers became more dispersed. Oligomers with a volume of less than 1000 $nm^3$ only after 2 h. This may seem counter-intuitive, but it is plausible that the smaller oligomers were not concentrated enough to be detected by nanopore detection. When fibrillar seeds were added, the oligomers were larger and more dispersed. The results revealed the formation of oligomers with a volume greater than 4000 $nm^3$ after 90 min of incubation, which were not detected in the control or with the addition of nonfibrous oligomers. This oligomer population was highly dispersed and consisted of a heterogeneous oligomer mixture. Regarding the addition of non-fibrillar seeds, species with a volume of less than 1000 $nm^3$ were detected at a later time, specifically after 60 min of incubation. This confirmed the role of the seed in promoting the formation of larger oligomers. The effect of seed morphology, specifically whether the oligomer and fiber were sonicated, has already been investigated using ThT fluorescence emission. It has been reported that sonication of fibers accelerates the aggregation process.[36] On the other hand, confocal fluorescence spectroscopy investigations have indicated that fibers are more seeding-competent than oligomers.[37] Similarly, our findings demonstrate that the aggregation process proceeds through the formation of large aggregates when small fibers are used as seeds. 4-Hydroxy-2-Nonenal is known to modify the structure of α-synuclein fibers, which raises the question of its effect on the size distribution of oligomers formed. Similarly, compared to previous experiments, a population of oligomers with a volume greater than 1000 $nm^3$ appeared earlier than in the control. This occurred after 30 min of incubation along with a population of smaller oligomers with a volume of less than 1000 $nm^3$. In this case, the results suggest that HNE fibers can accelerate the formation of large oligomers. However, they do not inhibit the formation of smaller α-synuclein seeds, as observed with spontaneously formed α-synuclein seeds (both fibrillar and non-fibrillar). Furthermore, although the seeds were fibrillar, we did not detect any oligomers with a volume greater than 4000 $nm^3$ within the first 360 min. For all conditions (seeded and control), we confirmed the presence of oligomers of comparable sizes by conducting TEM experiments at the end of the incubation time inside a nanopipette. Obviously, this confirmation does not allow for detailed analysis of the size distribution of the oligomers, as achieved by nanopore technology. This is because the low concentration and chemical treatment of the sample necessary to obtain the images can affect the accuracy of the results. Looking at the results as a whole, we observed that the volume distributions of the oligomers fluctuated with time for all experiments (control and seed). This phenomenon has been observed for Aβ peptides and α-synuclein.[29,30] This has been interpreted as the result of the different transient conformations that the oligomers take on over time before forming stable β-sheet structures. These structures adopt the most favorable conformation to form fibers. Interestingly, our results demonstrated that the addition of different types of seeds influences the morphology and formation times of oligomers.

## Conclusions

Our study aimed to investigate the influence of seeds on the volume of α-synuclein oligomers during early stages of aggregation. To achieve this, we present a geometric model that estimates the volume of detected aggregates based on the current blockade amplitude and pipette geometry (including diameter and angle). Our findings showed a significant agreement between the experimental values obtained through nanopores and microscopic analysis of oligomers produced using two different methods. This allowed us to directly map the species present during the initial stages of aggregation over time, and revealed that seeds induced the formation of larger oligomers compared to the control without seeds. Furthermore, fibrillar aggregates demonstrated better seed competency than fiber aggregates with HNE and oligomers. Overall, our study highlights the utility of nanopore technology for investigating the early stage aggregation kinetics. This technology provides information on oligomer size independent of specific structures, such as ThT. We believe that our findings open avenues for further investigations into amyloid growth and provide access to information on small oligomer sizes.

## Experimental Section

### Biochemistry

α-Synuclein monomers and oligomers were purchased from ND Biosciences (Lausanne, Switzerland). The solubilization of α-synuclein monomers in 1X PBS at 4 °C was performed according to a previously described protocol.[29] The concentration of the monomer solution was determined by measuring absorbance at 280 nm using a JASCO spectrophotometer. The solution was then aliquoted to a final concentration of 36 μM and stored at −80 °C until use.

To produce seeds, wild-type recombinant α-synuclein monomers (stock solution 58 μM in PBS 1X) were diluted to 50 μM in PBS in low-binding Eppendorf tubes and incubated at 37 °C without shaking to allow aggregation. After 6 and 23 h of incubation, the solutions were diluted in PBS to a concentration of 2 nM and stored at −80 °C until the seeding experiments. For microscopy of α-synuclein seeds and oligomers, samples were deposited onto Formvar carbon-coated grids, negatively stained with freshly filtered 2% uranyl acetate, and then dried. The TEM images were obtained using a JEOL 1400 electron microscope at an accelerating voltage of 80 kV.

### Pipette production and Characterization

Quartz capillaries were purchased from Sutter Instruments (ref Q100-30-7.5, OD: 1 mm & ID: 0.3 mm; ref Q100-50-10, OD: 1 mm & ID: 0.5 mm; and ref Q100-70-10, OD: 1 mm & ID: 0.7 mm). The capillaries were pulled using a P-2000 pipette puller (Sutter Instruments). The pulling parameters were chosen to achieve a tip diameter ranging from 10 to 60 nm (Table SI-1). After pulling the nanopipette, the surface was activated with O2 plasma at 100 W for 4 min at 20 sccm. The pipettes were then filled with pure degassed water using a thermally driven approach [32]. After complete filling, the nanopipettes were characterized using a 1 M NaCl solution and 1X PBS solution with a pH of 7.4. The nanopipette diameter ($r_p$) was determined using equation 1, which involves measuring the

conductance of a 1 M NaCl solution, PBS 1X pH 7.4, and the angle α determined by fluorescence microscopy (x1000) after filling it with a solution of Rhodamine G (Figure SI-1). A table of nanopipettes utilized in this study is provided in the Supporting Information.

$$r_p = \frac{G}{\kappa\pi\tan(\alpha) + 0.25} \quad (1)$$

where $\kappa$ is the conductivity of the electrolyte solution.

#### Resistive pulse experiments

The resistive pulse experiments were performed as follows: A solution containing α-synuclein was placed inside nanopipettes connected to the working electrode of an amplifier (EPC10 double or EPC10, HEKA, Germany). The ground electrode was placed in an external reservoir, and the detection experiment was conducted using a solution of 1 M NaCl, PBS 1X, with a pH of 7.4 at a temperature of 23 °C. A constant voltage was applied and the current was measured using a frequency of 200 kHz or 100 kHz, which was filtered with a Bessel filter at 10 kHz. The current traces were then analyzed using the custom-made LabVIEW software (PeakNanoTool). The signal was filtered using a Butterworth filter with a 5 kHz order of 1. Subsequently, the baseline fluctuations were corrected using a Savitzky-Golay filter of the order of 1. This correction was performed to establish a detection threshold of 6 σ, where σ represents the standard deviation of the baseline signal. These events were characterized by their relative blockade amplitudes (ΔImax/I). Statistical analyses were performed using a custom MATLAB script.

For the analysis, 500 nM α-synuclein oligomers (ND Biosciences, Lausanne, Switzerland) in 1 M NaCl (containing 1X PBS, pH 7.4) was added directly to the pipette. A voltage of +500 mV or −500 mV was applied.

For the seeding experiments, monomers were diluted to a concentration of 100 nM in NaCl 1 M (containing PBS 1X, pH 7.4). These diluted monomers were then added directly into the pipette, either without seeds or with seeds, at an equivalent monomer concentration of 200 pM. The experiment consisted of two phases. First, a voltage of 500 mV was applied for 7.5 min, followed by a voltage of −500 mV for the same duration. During this experiment, the current was measured using an EPC10 amplifier (HEKA, Lambrecht, Germany) at sampling rates of 200 kHz or 100 kHz. The signal was filtered using a Bessel filter set at 10 kHz. The second phase was a 15-minute break without an applied voltage. This process was repeated for 6 h to incubate the α-synuclein inside the pipette. The data were analyzed every 30-minute cycle to obtain kinetic information.

## Supporting Information

The authors have cited additional references in the Supporting Information. Additional data on nanopipette production and characterization, lists of nanopipettes used in this work, TEM images of α-synuclein oligomers SP and DA, evolution of current trace recorded over the incubation time and TEM images of α-synuclein oligomers obtained after 6H of incubation inside a nanopipette without and with different preformed seeds.

## Acknowledgements

This work was funded by the Michael J Fox Foundation for Parkinson's Research (grant ID: MJFF-021093).

## Conflict of Interests

The authors declare no conflict of interest.

## Data Availability Statement

The data that support the findings of this study are available from the corresponding author upon reasonable request.

**Keywords:** nanopore · nanopipette · aggregation · α-synuclein

[1] a) S. Mukherjee, A. Sakunthala, L. Gadhe, M. Poudyal, A. S. Sawner, P. Kadu, S. K. Maji, *J. Mol. Biol.* **2023**, *435*, 167713; b) D. Snead, D. Eliezer, *Exp. Neurobiol.* **2014**, *23*, 292.
[2] F. Castello, J. M. Paredes, M. J. Ruedas-Rama, M. Martin, M. Roldan, S. Casares, A. Orte, *Sci. Rep.* **2017**, *7*, 40065.
[3] G. K. Tofaris, *Cellular and molecular life sciences* **2022**, *79*, 210.
[4] E. Zurlo, P. Kumar, G. Meisl, A. J. Dear, D. Mondal, M. M. A. E. Claessens, T. P. J. Knowles, M. Huber, *PLoS One* **2021**, *16*, e0245548.
[5] A. K. Buell, C. Galvagnion, R. Gaspar, E. Sparr, M. Vendruscolo, T. P. J. Knowles, S. Linse, C. M. Dobson, *Proc. Natl. Acad. Sci. USA* **2014**, *111*, 7671.
[6] V. Gupta, S. Salim, I. Hmila, N. N. Vaikath, I. P. Sudhakaran, S. S. Ghanem, N. K. Majbour, S. A. Abdulla, M. M. Emara, H. B. Abdesselem et al, *Sci. Rep.* **2020**, *10*, 8137.
[7] L. Pieri, K. Madiona, R. Melki, *Sci. Rep.* **2016**, *6*, 24526.
[8] T. Ibrahim, J. McLaurin, *Biochem. Biophys. Res. Commun.* **2016**, *469*, 529.
[9] G. Tanaka, T. Yamanaka, Y. Furukawa, N. Kajimura, K. Mitsuoka, N. Nukina, *Biochim. Biophys. Acta Mol. Basis Dis.* **2019**, *1865*, 1410.
[10] E.-J. Bae, D.-H. Ho, E. Park, J. W. Jung, K. Cho, J. H. Hong, H.-J. Lee, K. P. Kim, S.-J. Lee, *Antioxid. Redox Signaling* **2013**, *18*, 770.
[11] H. Yagi, E. Kusaka, K. Hongo, T. Mizobata, Y. Kawata, *J. Biol. Chem.* **2005**, *280*, 38609.
[12] X.-Y. Du, X.-X. Xie, R.-T. Liu, *Int. J. Mol. Sci.* **2020**, *21*.
[13] B. R. Groveman, C. D. Orrù, A. G. Hughson, L. D. Raymond, G. Zanusso, B. Ghetti, K. J. Campbell, J. Safar, D. Galasko, B. Caughey, *Acta Neuropathologica Communications* **2018**, *6*, 7.
[14] L. Alvarez-Erviti, Y. Seow, A. H. Schapira, C. Gardiner, I. L. Sargent, M. J. A. Wood, J. M. Cooper, *Neurobiol. Dis.* **2011**, *42*, 360.
[15] a) C. Cao, P. Magalhães, L. F. Krapp, J. F. Bada Juarez, S. F. Mayer, V. Rukes, A. Chiki, H. A. Lashuel, M. Dal Peraro, *ACS nano* **2023**; b) K.-L. Xin, Z.-L. Hu, S.-C. Liu, X.-Y. Li, J.-G. Li, H. Niu, Y.-L. Ying, Y.-T. Long, *Angew. Chem. Int. Ed.* **2022**, *61*, e202209970; c) H.-Y. Wang, Z. Gu, C. Cao, J. Wang, Y.-T. Long, *Anal. Chem.* **2013**, *85*, 8254; d) M. Afshar Bakshloo, S. Yahiaoui, M. Bourderioux, R. Daniel, M. Pastoriza-Gallego, J. J. Kasianowicz, A. Oukhaled, *ACS Chem. Neurosci.* **2023**, *14*, 2517.
[16] J. Houghtaling, J. List, M. Mayer, *Small* **2018**, *14*, e1802412.
[17] N. Meyer, I. Abrao-Nemeir, J.-M. Janot, J. Torrent, M. Lepoitevin, S. Balme, *Adv. Colloid Interface Sci.* **2021**, *298*, 102561.
[18] S. Awasthi, C. Ying, J. Li, M. Mayer, *ACS Nano* **2023**, *17*, 12325.
[19] R. Hu, J. Diao, J. Li, Z. Tang, X. Li, J. Leitz, J. Long, J. Liu, D. Yu, Q. Zhao, *Sci. Rep.* **2016**, *6*, 20776.
[20] a) I. Abrao-Nemeir, J. Bentin, N. Meyer, J.-M. Janot, J. Torrent, F. Picaud, S. Balme, *Chem. Asian J.* **2022**, *17*, e202200726; b) X. Li, X. Tong, W. Lu, D. Yu, J. Diao, Q. Zhao, *Nanoscale* **2019**, *11*, 6480.
[21] N. Meyer, N. Arroyo, J.-M. Janot, M. Lepoitevin, A. Stevenson, I. A. Nemeir, V. Perrier, D. Bougard, M. Belondrade, D. Cot et al, *ACS Sens.* **2021**, *6*, 3733.
[22] I. Abrao-Nemeir, N. Meyer, A. Nouvel, S. Charles-Achille, J.-M. Janot, J. Torrent, S. Balme, *Biophys. Chem.* **2023**, *300*, 107076.

[23] N. Giamblanco, D. Coglitore, A. Gubbiotti, T. Ma, E. Balanzat, J.-M. Janot, M. Chinappi, S. Balme, *Anal. Chem.* **2018**, *90*, 12900.
[24] N. Martyushenko, N. A. W. Bell, R. D. Lamboll, U. F. Keyser, *Analyst* **2015**, *140*, 4882.
[25] N. Giamblanco, Y. Fichou, J.-M. Janot, E. Balanzat, S. Han, S. Balme, *ACS Sens.* **2020**, *5*, 1158.
[26] R.-J. Yu, S.-M. Lu, S.-W. Xu, Y.-J. Li, Q. Xu, Y.-L. Ying, Y.-T. Long, *Chem. Sci.* **2019**, *10*, 10728.
[27] C. C. Chau, S. E. Radford, E. W. Hewitt, P. Actis, *Nano Lett.* **2020**, *20*, 5553.
[28] N. Giamblanco, J.-M. Janot, A. Gubbiotti, M. Chinappi, S. Balme, *Small Methods* **2020**, *4*, 1900703.
[29] N. Meyer, J.-M. Janot, J. Torrent, S. Balme, *ACS Cent. Sci.* **2022**, *8*, 441.
[30] N. Meyer, J. Bentin, J.-M. Janot, I. Abrao-Nemeir, S. Charles-Achille, M. Pratlong, A. Aquilina, E. Trinquet, V. Perrier, F. Picaud et al, *Anal. Chem.* **2023**, *95*, 12623.
[31] S. T. Kumar, S. Donzelli, A. Chiki, M. M. K. Syed, H. A. Lashuel, *J. Neurochem.* **2020**, *153*, 103.
[32] M. Firnkes, D. Pedone, J. Knezevic, M. Döblinger, U. Rant, *Nano Lett.* **2010**, *10*, 2162.
[33] R. W. DeBlois, C. P. Bean, *Rev. Sci. Instrum.* **1970**, *41*, 909.
[34] Y. Cai, C. Lendel, L. Österlund, A. Kasrayan, L. Lannfelt, M. Ingelsson, F. Nikolajeff, M. Karlsson, J. Bergström, *Biochem. Biophys. Res. Commun.* **2015**, *464*, 336.
[35] a) T. T. Ding, S.-J. Lee, J.-C. Rochet, P. T. Lansbury, *Biochemistry* **2002**, *41*, 10209; b) M. M. Apetri, N. C. Maiti, M. G. Zagorski, P. R. Carey, V. E. Anderson, *J. Mol. Biol.* **2006**, *355*, 63.
[36] A. Sakunthala, D. Datta, A. Navalkar, L. Gadhe, P. Kadu, K. Patel, S. Mehra, R. Kumar, D. Chatterjee, J. Devi, et al., *J. Phys. Chem. Lett.* **2022**, *13*, 6427.
[37] D. Lau, C. Magnan, K. Hill, A. Cooper, Y. Gambin, E. Sierecki, *ACS Chem. Neurosci.* **2022**, *13*, 883.

Manuscript received: November 1, 2023
Revised manuscript received: January 18, 2024
Accepted manuscript online: January 19, 2024
Version of record online: February 2, 2024